

PointLoc: Deep Pose Regressor for LiDAR Point Cloud Localization

Wei Wang¹ Bing Wang¹
 Ronald Clark² Bo Yang¹
¹University of Oxford

Peijun Zhao¹ Changhao Chen¹
 Andrew Markham¹ Niki Trigoni¹
²Imperial College London

Abstract

In this paper, we present a novel end-to-end learning-based LiDAR relocalization framework, termed PointLoc, which infers 6-DoF poses directly using only a single point cloud as input, without requiring a pre-built map. Compared to RGB image-based relocalization, LiDAR frames can provide rich and robust geometric information about a scene. However, LiDAR point clouds are unordered and unstructured making it difficult to apply traditional deep learning regression models for this task. We address this issue by proposing a novel PointNet-style architecture with self-attention to efficiently estimate 6-DoF poses from 360° LiDAR input frames. Extensive experiments on recently released challenging Oxford Radar RobotCar dataset and real-world robot experiments demonstrate that the proposed method can achieve accurate relocalization performance.

1. Introduction

LiDAR-based relocalization methods have achieved impressive accuracy [13, 15, 17]. A typical LiDAR relocalization system usually includes a feature extraction module, a feature matching algorithm, an outlier rejection step, a matching cost function, a spatial searching or optimization method and a temporal optimization or filtering mechanism [22]. Although these geometric localization methods achieve high accuracy in some scenarios, they require significant hand-engineering efforts to tune the huge amount of hyper-parameters, and depend heavily on the running environments.

A number of novel map-based approaches have been proposed to estimate global poses [2, 4, 18, 22, 34, 40]. For example, Barsan and Wang *et al.* [2] proposed to learn descriptors from LiDAR intensity, and relocalization was performed by matching descriptors against pre-built intensity maps. However, although these methods achieve considerable accuracy, it is hard to build the map and the computing complexity increases greatly when the map gets larger. Additionally, they require other systems to provide an accurate initial pose as coarse localization first.

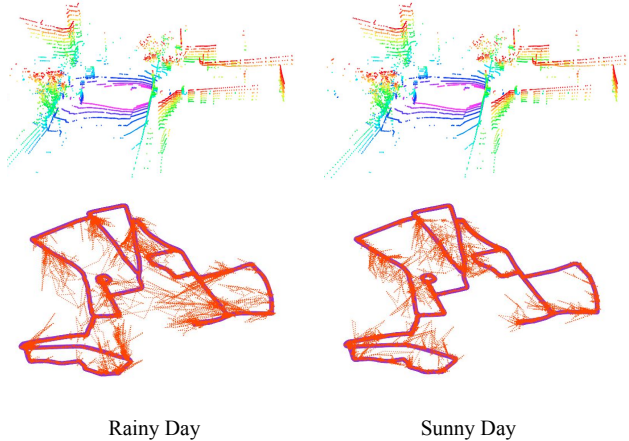


Figure 1. PointLoc results for the challenging Oxford Radar RobotCar dataset [1, 23]. We directly feed the LiDAR point cloud from a single timestamp to the neural network for predicting the 6-DoF pose without the requirement of pre-built maps. The estimations of PointLoc are robust regardless of weather, and outperform the state-of-the-art DNN-based LiDAR and visual relocalization methods significantly.

Thus, most localization solutions employ Global Navigation Satellite System (GNSS) to provide pose estimations. Unfortunately, GNSS is not always available such as in indoor environments and the accuracy of GNSS cannot be guaranteed in areas like large cities where high-rising buildings can block the GNSS signals. To this end, Uy *et al.* [31] proposed a point cloud retrieval-based localization method to deal with the situation when the GNSS is absent. It obtains a 6-DoF pose with respect to the pre-built map in the form of reference database. Dube *et al.* [7] further proposed SegMap to improve the storage efficiency of the reference database by storing data-driven descriptors of individual objects in a point cloud. However, retrieval-based approaches inherently suffer from several issues. First, the time complexity of finding the closest match between the query point cloud and the reference point cloud is $O(n)$ where n is the number of point clouds, which is not suitable for common real-time application scenarios. Second, the point cloud-based method requires a reference database, which occu-

pies $O(n)$ storage space and cannot be deployed on many mobile robots. Third, the recall rate of it is often not good enough [31].

Recently, learning-based approaches have emerged as a promising tool to build up a completely end-to-end localization system. These methods do not require any reference databases during runtime, and the learned features tend to be general and robust. These kind of localization approaches train a neural network to directly predict the pose. Their time complexity during inference time is $O(1)$ and the space it occupies is only the model size, which addresses the drawbacks of point cloud retrieval-based methods. Early attempts in this direction include PoseNet and its variations [5, 11, 12, 30]. However, all the current pose regression approaches utilize RGB images as inputs, which have several problems. Visual inputs are sensitive to the change of environments, resulting in suboptimal localization performance. In addition, the input images are restricted to a narrow Field-of-View (FoV). These aspects restrict the application of these approaches to the real world. Compared with RGB images, point clouds, acquired by LiDAR, capture 360° 3-D space, and provide much richer geometric information of a specific location. In addition, the features extracted from point clouds tend to be more robust compared to those extracted from images. However, point clouds are unordered and unstructured, making it difficult to learn features for localization. Motivated by this, we design a neural network to use LiDAR point clouds as input for robust and accurate localization.

In this paper, we propose a novel neural network-based 3-D pose regressor, named PointLoc, to accurately estimate the 6-DoF pose using LiDAR point clouds. The neural network directly takes a primitive point cloud as input and estimates the 6-DoF pose in an end-to-end fashion. The performance shows significant improvement over the learning-based LiDAR point cloud and camera relocalization methods. Fig. 1 illustrates the superior performance of our PointLoc approach in different environments found in the Oxford Radar RobotCar dataset.

In summary, our contributions are as follows:

- To the best of our knowledge, this is the first LiDAR point cloud-based approach for deep global pose regression in an end-to-end fashion. Our proposed architecture with a self-attention module can further improve the accuracy of the predicted 6-DoF absolute poses.
- We conduct real-world robot experiments in an indoor environment. We will release the collected indoor LiDAR-image dataset dubbed vReLoc for studying the indoor relocalization task.
- Comprehensive experiments and an ablation study on these two new datasets have been done to evaluate

our proposed method. Results demonstrate that the PointLoc model outperforms the state-of-the-art DNN-based LiDAR point cloud and visual relocalization methods by a large margin.

2. Related Works

In this section, we review different learning-based approaches for relocalization, LiDAR Odometry which estimates ego-motions between consecutive point clouds, and DNN architectures on point clouds.

2.1. Camera Relocalization

For dealing with the drawbacks of map registration methods, recent works propose learning-based approaches to estimate the global pose directly [3, 5, 8, 9, 11, 12, 24, 25, 29, 32, 33, 41]. They take images, either single or sequential, as inputs to train a neural network model for predicting absolute poses. The key to these methods is to learn a deep pose regressor, which usually comprises a feature extractor and a regressor [9, 12, 35]. For example, PoseNet related works [10–12] proved the feasibility of predicting the global pose using a single RGB image by regressing the pose directly. Brahmbhatt *et al.* [3] utilized the relative pose between two images as a geometric constraint to estimate the pose. Huang *et al.* [9] and Wang *et al.* [35] have demonstrated that self-attention modules can significantly improve the accuracy of relocalization and guide the network to ignore distracting information from foreground objects in a dynamic environment. Although DNN-based relocalization methods can solve the downsides of retrieval-based approaches, the performance of translation and rotation estimation is still not satisfactory enough to be applied to real-world scenarios [30], which calls for further work on learning algorithms. Our work follows this line of study, aiming to improve the accuracy of deep global pose regression.

2.2. DNN-based LiDAR Odometry

Recent works propose learning-based methods to estimate LiDAR Odometry, which calculates relative poses between consecutive LiDAR scans. Wang *et al.* [37] proposed a deep parallel neural network to directly predict relative poses. 3DFeat-Net [43] was developed to learn both 3-D feature detector and descriptor for point cloud matching using weak supervision. Lu *et al.* [21] proposed a Virtual Corresponding Points method to align two point clouds accurately. Wang *et al.* [38] designed novel sub-network architectures to address difficulties in the ICP method. These point cloud registration approaches can be leveraged to predict LiDAR Odometry. However, different from these methods, our work focuses on relocalization, which estimates global poses rather than relative poses.

2.3. Deep Learning on Point Clouds

DNN-based feature extraction methods for point clouds [16, 26–28] have gained significant success in recent years. VoxelNet [45] was developed to learn feature embeddings in voxels for object detection. PointNet++ related works [26–28] have been proposed to directly process unordered point sets and learn features from points, which showed impressive performance on tasks of 3-D object detection, part segmentation, and semantic segmentation. Detailed introductions and applications of deep learning for point clouds can be found in the recent survey paper [19].

3. Problem Statement

We design a DNN-based framework for performing deep global pose regression using point cloud data from a LiDAR sensor. We predict the absolute 6-DoF poses of the mobile agent within previously visited areas. A typical use case for our method would be when a mobile agent has already visited the query places before, and then has to localize itself again when it moves across the previously-visited environment. To enable a more generic and reliable relocalization system, we only consider one LiDAR input at a single timestamp rather than sequential inputs.

For each timestamp t , the agent receives one point cloud frame $\mathbf{P}_t = \{\mathbf{x}_i \mid i = 1, \dots, N\}$ from LiDAR, where each point \mathbf{x}_i is a vector of describing its coordinate (x, y, z) . Therefore, the shape for each \mathbf{P}_t is $(N, 3)$. The relocalization of the agent is parameterized by a 6-DoF pose $[\mathbf{t}, \mathbf{r}]^T$ with respect to the world coordinate, where $\mathbf{t} \in \mathbb{R}^3$ is a 3-D translation vector and $\mathbf{r} \in \mathbb{R}^4$ is a 4-D rotation vector (quaternion). To this end, deep 3-D pose regressors learn a function \mathcal{F} such that $\mathcal{F}(\mathbf{P}_t) = [\mathbf{t}, \mathbf{r}]^T$, where the function \mathcal{F} is usually a neural network for DNN-based methods.

4. Deep Point Cloud Relocalization

This section introduces our proposed PointLoc, a deep 3-D pose regressor for predicting the global pose from point cloud data. The overall architecture is illustrated in Fig. 2. Our model consists of a point cloud encoder, a self-attention module, group all layers, and a pose regressor. The point cloud data are down-sampled to a fixed shape $(N, 3)$ as an input. The whole design is based on the PointNet-style structure, which can theoretically learn a critical subset of points for relocalization.

4.1. Point Cloud Pre-Processing

Each point cloud frame of a LiDAR scan contains a different number of points. However, our neural network requires the same point cloud dimensions $(N, 3)$ for its inputs. To tackle this problem, we adopt the random point cloud sampling strategy. We ensure that all the point cloud inputs have the same shape $(N, 3)$. N is set to 20,480 in this work.

4.2. Point Cloud Feature Encoder

The feature representation extracted by the point cloud encoder plays a critical role in achieving accurate and reliable relocalization. Intuitively, human beings can utilize key points and features in a scene to identify where they are and conventional geometric methods are capable of performing precise localization by exploiting key points of the point cloud data. Inspired by this, if a neural network learns a subset of key points from the original point cloud data relevant to the localization task, we can take better advantage of these key features to identify a location. Existing literature [27, 44] has proved the critical-subset theory, i.e. for any point cloud \mathbf{P} , a PointNet-like structure can identify a salient point subset $\mathbf{C} \subseteq \mathbf{P}$, making it a desirable choice for our relocalization task.

Specifically, PointNet exploits the multi-layer perceptron (MLP), feature transformation module, and max pooling layer to approximate a permutation invariant function for point cloud classification and segmentation. In fact, it is a universal continuous set function approximator, described as:

$$f(x_1, \dots, x_N) = \phi(\mathbf{MAX}\{h(x_i) \mid x_i \in \mathbf{P}\}) \quad (1)$$

where ϕ and h are two continuous functions (they are usually instantiated to be an MLP), and \mathbf{MAX} denotes the max pooling layer [28]. PointNet++ extends PointNet by recursively capturing the hierarchical features on point sets in a metric space [28]. From the aforementioned Eq. 1, the result of the PointNet structure is determined by $u = \mathbf{MAX}\{h(x_i) \mid x_i \in \mathbf{P}\}$, and the \mathbf{MAX} operation takes N vectors as input and outputs one vector of element-wise maximums. Thus, there exists one $x_i \in \mathbf{P}$ such that $u_j = h_j(x_i)$, where u_j is the j^{th} dimension of u , and μ_j is the j^{th} dimension of $h(x_i)$. These points can be aggregated into a critical subset $\mathbf{C} \subseteq \mathbf{P}$, where \mathbf{C} determines u and then $\phi(u)$ (more details can be found in [27, 44]). Consequently, the critical-subset theory is applicable to neural networks of the structure of $\phi(\mathbf{MAX}\{h(x_i) \mid x_i \in \mathbf{P}\})$. The proposed PointLoc is built upon PointNet++, consisting of such a structure and thus can learn the critical subset from LiDAR point clouds in theory.

4.3. Self-Attention for Robust Relocalization

Prior works [9, 35] have proved that the self-attention mechanism can improve camera relocalization by removing noisy features. Therefore, we also design a neural module to automatically remove the dynamic features before regressing the final poses. Inspired by the recent works [9, 35, 42], we introduce a self-attention module to learn a mask.

Given a set of point features $\mathbf{F} \in \mathbb{R}^{N \times C}$ which are learned from the point cloud encoder, our attention module aims to learn a mask $M \in \mathbb{R}^{1 \times C}$ for the features \mathbf{F} . To achieve this, we use a shared MLP followed by a *sigmoid* function to

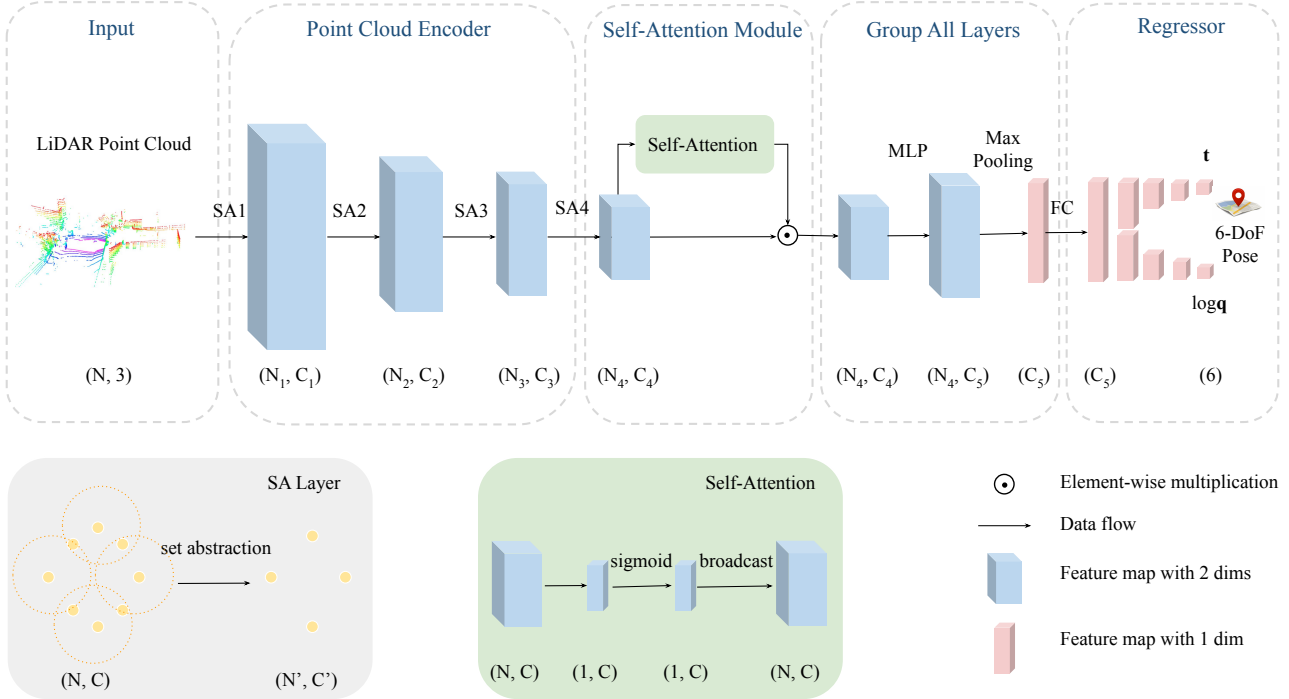


Figure 2. The architecture of PointLoc. It consists of a point cloud encoder, a self-attention module, a grouping all (GA) layers module and a pose regressor. The encoder is composed of 4 consecutive set abstraction (SA) layers. Each SA layer shown in the diagram [20] consists of a sampling layer, a grouping layer and a PointNet layer [27]. The learnt point features are sent to self-attention module for eliminating the noisy features. Afterwards, these features are fed into group all (GA) layers for down-sampling to a feature vector. Finally, the pose regressor takes the feature vector as input and then regresses the 6-DoF Pose.

take the features \mathbf{F} as input and then directly generate the mask M . After that, we broadcast and mask the features \mathbf{F} by M , obtaining weighted features $\hat{\mathbf{F}}$ for subsequent pose regression. Formally, this self-attention module is defined as follows:

$$\hat{\mathbf{F}} = \mathbf{F} \cdot M \quad (2)$$

4.4. The Architecture of PointLoc

Accurate relocalization requires scene perception and geometric reasoning. The proposed PointLoc consists of a point cloud encoder, a self-attention module, grouping all (GA) layers and a pose regressor as shown in Fig. 2. Instead of extracting point cloud features by hand-crafted methods, we designed a point cloud encoder based on the set abstraction (SA) layer of PointNet++ [26, 28] as discussed before. The point cloud encoder is composed of 4 consecutive SA layers. Each SA layer is composed of a sampling layer, a grouping layer and a PointNet layer [27]. The SA layer takes a feature matrix $\mathbf{F} \in R^{N \times C}$ as input where N is the point number and C is the feature dimension of each point, and outputs a feature matrix $\mathbf{F}' \in R^{N' \times C'}$ where N' is the sub-sampled point number and C' is the new feature dimension of each point (from the size (N_1, C_1) to (N_4, C_4) in Fig. 2).

We also leverage multi-scale grouping strategy [28] inside the SA layer for robust feature learning. Specifically, the layer adopts farthest point sampling to sample N' regions with x_j being the region centers, and for each region with radius r , it extracts local features with a symmetric function as [20]:

$$\mathbf{F}'_j = \text{MAX}_{\{i \mid \|x_i - x_j\| \leq r\}} \{h(\mathbf{F}_i, x_i - x_j)\} \quad (3)$$

where \mathbf{F}_i is the i^{th} row of \mathbf{F} , \mathbf{F}'_j is the j^{th} row of \mathbf{F}' , $h: R^C \rightarrow R^{C'}$ is the MLP, and MAX is the max pooling layer. After the last SA layer of the point cloud encoder, we apply a point self-attention module, which intends to learn a probability distribution to filter out features from outliers for better relocalization performance. Afterwards, the GA layer aggregates point features from all previous layers to generate an embedded feature vector. Specifically, shown in Fig. 2, the input of the GA layer is a point feature set of size $N_4 \times C_4$, and then the point features are propagated to an updated point feature set of size $N_4 \times C_5$ via MLP, where C_5 is larger than C_4 . Next, it is down-sampled to the C_5 dimension feature vector through the max pooling layer. The embedded feature vector is then forwarded to an FC layer. After the FC layer, the C_5 dimensional feature vector

is finally sent to the pose regressor for predicting the translation \mathbf{t} and rotation \mathbf{r} respectively. The pose regressor is composed of consecutive FC layers.

4.5. Loss Function

Our goal is to estimate the 6-DoF pose $[\mathbf{t}, \mathbf{r}]^T$. Prior works [5, 6, 11, 12] directly predict quaternions and use an l_1 or l_2 loss, but such a representation is over-parameterized and normalization of the output quaternion is required at the cost of worse accuracy [3]. Odometry tasks with DNNs [36, 37] usually regress Euler angles, which are also not suitable here since they wrap around 2π . Consequently, we employ the definition of the loss function in [3] for training our neural network, which is adapted from [11]. Given K training samples $\mathcal{G} = \{\mathbf{P}_t \mid t = 1, \dots, K\}$ and their corresponding ground-truth poses $\{\hat{\mathbf{t}}, \hat{\mathbf{r}}_t^T \mid t = 1, \dots, K\}$, the parameters of the PointLoc are learned via the following loss function:

$$\mathcal{L}(\mathcal{G}) = \|\mathbf{t} - \hat{\mathbf{t}}\|_1 e^{-\beta} + \beta + \|\log \mathbf{q} - \log \hat{\mathbf{q}}\|_1 e^{-\gamma} + \gamma \quad (4)$$

where β and γ are balanced factors to jointly learn translation and rotation. It is worth noting that the β and γ are learnable factors during training, which are initialized by β^0 and γ^0 respectively. $\log \mathbf{q}$ is the logarithmic form of a unit quaternion $\mathbf{q} = (u, \mathbf{v})$, where u is a scalar and \mathbf{v} is a 3-D vector. It is defined as:

$$\log \mathbf{q} = \begin{cases} \frac{\mathbf{v}}{\|\mathbf{v}\|} \cos^{-1} u, & \text{if } \|\mathbf{v}\| \neq 0 \\ \mathbf{0}, & \text{otherwise} \end{cases} \quad (5)$$

5. Indoor LiDAR Relocalization Dataset

There is a lack of public datasets in the indoor environment with point cloud data. In order to boost the research in this area, we collected a new dataset dubbed vReLoc with rich sensor modalities, e.g. vision and LiDAR data on a mobile robot platform. Our dataset will be released to benefit future researchers.

The experimental robot is Turtlebot 2, mounted with a Velodyne HDL-32E LiDAR and an Intel RealSense Depth Camera D435. The sensors have been carefully calibrated. The Velodyne is a lightweight pulsed laser for Detection and Ranging, which features 32 lasers across over a 40° vertical field-of-view and a 360° horizontal field-of-view. It runs at a frequency of 10Hz. Each point cloud in the dataset contains $\sim 60,000$ points. The camera was employed to capture RGB images, and the size of each image is $640 \times 480 \times 3$. A Vicon Motion Tracker system is leveraged for acquiring accurate ground truth 6-DoF poses. 10 Bonita B10 cameras are used in the system, installed around the area where the dataset is collected. Each Bonita B10 has the resolution of 1 megapixel with 250 fps frame rate, and an operating range of up to 13 m. The system can track the pose of the robot at a precision of $\sim 1\text{cm}$.

Table 1. Dataset Descriptions on the vReLoc.

| Sequence | Scenario | Training | Test |
|------------------------|---------------------|----------|------|
| Seq-03 | static | ✓ | |
| Seq-12, Seq-15 | one-person walking | ✓ | |
| Seq-16 | two-persons walking | ✓ | |
| Seq-05, Seq-06, Seq-07 | static | | ✓ |
| Seq-14 | one-person walking | | ✓ |

The size of the Vicon room is about $4m \times 5m$. We lay out several obstacles in the scene. For the relocalization task, the scene is fixed through the whole data collection process. We utilized the Robot Operating System (ROS) for robot control and data collection. Timestamps were recorded on every frame of each sensor by the ROS, and we synchronized world timestamp across different systems from the same Network Time Protocol (NTP) server.

A total of 18 sequences were collected of various lengths. Since the Velodyne LiDAR, RealSense camera and Vicon motion tracker system run in different frequencies, we synchronized these systems so that the image and LiDAR in each timestamp has the same 6-DoF pose. For the static scenario, there are no moving objects in the scene. For other scenarios, there are people randomly walking in the scene. Sequences 01-10 come from the static environment, sequences 11-15 are the one-person moving scenario, and sequences 16-18 are two-persons moving scenario. In order to better represent real-world situations, in our experiments, we specially chose challenging sequences as the training dataset. We report our training and test sequences from the vReLoc dataset in Table 1.

6. Experiments

In this section, we evaluate our proposed approach on the recently released outdoor Oxford Radar RobotCar [1, 23] dataset and our proposed indoor vReLoc dataset and compare to state-of-the-art methods.

6.1. Implementation Details

Adam [14] is applied to train our network with $\beta_1 = 0.9$ and $\beta_2 = 0.999$. We set the initial values $\beta_0 = 0.0$ and $\gamma_0 = -3.0$ of the loss function. The learning rate is set to 0.001, and we train 100 epochs on both datasets. For baseline image approaches, we also used data augmentation to improve the accuracy of predictions. Following the convention of existing works [3, 11, 12, 30, 35], we calculate the mean error for outdoor datasets and the median error for indoor datasets.

The parameter settings of the point cloud encoder is shown in Table 2. In Table 3, we present the parameter settings of the self-attention module. The parameter setting of the group all layers is shown in Table 4. We show the parameter setting of the pose regressor in Table 5.

Table 2. Parameter Setting of the Point Cloud Encoder.

| Layer Name | Point Num | Radius | Sample Num | MLP |
|------------|-----------|--------|------------|----------------------|
| SA1 | 2048 | 0.2 | 64 | [0, 64, 64, 128] |
| SA2 | 1024 | 0.4 | 32 | [128, 128, 128, 256] |
| SA3 | 512 | 0.8 | 16 | [256, 128, 128, 256] |
| SA4 | 256 | 1.2 | 16 | [256, 128, 128, 256] |

Table 3. Parameter Setting of the Self-Attention Module.

| Layer Name | Point Dimension | Feature Dimension |
|-----------------------|-----------------|-------------------|
| Self-Attention Module | 256 | 256 |

Table 4. Parameter Setting of the Group All Layers.

| Layer Name (Ignore Max Pooling Layer) | Feature Dimension |
|---------------------------------------|-----------------------|
| Multi-Layer Perceptron (MLP) | [256, 256, 512, 1024] |
| Fully-Connected Layer (FC) | 1024 |

Table 5. Parameter Setting of the Pose Regressor. \mathbf{t} branch and $\log \mathbf{q}$ branch share the same parameter setting.

| Layer Name | Feature Dimension | LeakyReLu |
|-----------------|-------------------|-----------|
| FC1 + LeakyReLu | [1024, 512] | 0.2 |
| FC2 + LeakyReLu | [512, 128] | 0.2 |
| FC3 + LeakyReLu | [128, 64] | 0.2 |
| FC4 | [64, 3] | NA |

6.2. Baselines

To validate the performance of the proposed PointLoc, we compare it with several state-of-the-art learning-based LiDAR localization and camera relocalization approaches. For LiDAR localization approaches, we choose PointNetVLAD [31] and Deep Closest Point (DCP) [38]. PointNetVLAD is a large-scale point cloud retrieval-based approach, which can be utilized for LiDAR relocalization. We create the triplet training dataset, increase the point number from 4,096 to 8,192, and set the loss margin from 0.5 to 1.0 to improve the performance, while other hyper-parameters are kept the same as the vanilla PointNetVLAD. The validation sequence FULL 5 is chosen for building up the reference database as the localization map. DCP is a DNN-based point cloud registration approach, which employs the PointNet [27] and DGCNN [39] as the embedding network, and we adapt it for relocalization. For the camera relocalization baselines, we choose PoseNet17 [11] since it outperforms PoseNet and Bayesian PoseNet in previous works. AtLoc [35] is selected for comparison since it is the state-of-the-art single image-based learning approach. We also choose LSTM-Pose [33] as the sequential baseline. Moreover, we also compare with MapNet [3] because it is the state-of-the-art sequential image approach. We note that sequential methods generally perform better than single image ones by utilizing time constraints. However, for the relocalization task, this past information is not always

Table 6. Dataset Descriptions on the Oxford Radar RobotCar.

| Scene | Time | Tag | Training | Validation | Test |
|-------|---------------------|----------|----------|------------|------|
| FULL1 | 2019-01-11-14-02-26 | sun | ✓ | | |
| FULL2 | 2019-01-14-12-05-52 | overcast | ✓ | | |
| FULL3 | 2019-01-14-14-48-55 | overcast | ✓ | | |
| FULL4 | 2019-01-18-15-20-12 | overcast | ✓ | | |
| FULL5 | 2019-01-15-14-24-38 | overcast | | | ✓ |
| FULL6 | 2019-01-10-11-46-21 | rain | | | ✓ |
| FULL7 | 2019-01-15-13-06-37 | overcast | | | ✓ |
| FULL8 | 2019-01-17-14-03-00 | sun | | | ✓ |
| FULL9 | 2019-01-18-14-14-42 | overcast | | | ✓ |

available as discussed before. We still compare with them to examine how competitive our method is. We note that we implement baseline methods and tune them for the best performance.

6.3. Results on the Oxford Radar RobotCar

The Oxford Radar RobotCar dataset [1] is a radar extension to the Oxford RobotCar dataset [23], providing data from dual Velodyne HDL-32E LiDARs and Grasshopper2 monocular cameras. The ground truth poses are obtained by a NovAtel SPAN-CPT ALIGN inertial and GPS navigation system (GPS/INS).

Dataset Description The data were gathered in January 2019 over thirty-two traversals of a central Oxford route, and the duration and distance of each traversal are ~ 32 mins and ~ 9.05 km respectively. The resolution of a captured RGB image is 1280×960 , and each point cloud has $\sim 21,000$ points. We observe that the dataset is large-scale, covers various weather conditions and has moving objects like people and cars in the scenes, all of which have significant influence on the accuracy of relocalization task, and therefore it is quite challenging. Since there is a timestamp misalignment between camera and LiDAR sensors, we synchronize timestamps with scripts and interpolate (GPS/INS) measurements to coincide with the ground truth poses. We report the training and test sequences we used from the Oxford Radar RobotCar in Table 6.

Results The test results of the Radar RobotCar are presented in Table 7. Following the plotting style of relocalization work [9], the trajectories of FULL7 and FULL8 of DCP, MapNet, AtLoc, and PointLoc are shown in Fig. 3. PointLoc is much better than the LiDAR point cloud retrieval-based approach PointNetVLAD in terms of accuracy, which proves the effectiveness of our proposed network. As seen from Table 8, PointLoc can satisfy real-time operation and the storage space is small. The inference time is around 0.1sec, which means that by using this system, the real-time localization is achievable at 10 Hz. This indicates that PointLoc is better than existing point cloud retrieval-based approaches for relocalization. Moreover, PointLoc outperforms DCP significantly, which reveals that the proposed embedding neural network can ef-

Table 7. Mean translation error (m) and rotation error ($^{\circ}$) for the state-of-the-art methods on the Oxford Radar RobotCar.

| Scene | PointNetVLAD [31] | DCP [38] | PoseNet17 [11] | LSTM-Pose [33] | MapNet [3] | AtLoc [35] | PointLoc (Ours) |
|---------|-------------------------|-------------------------|---------------------------|-------------------------|-------------------------|-------------------------|--|
| FULL6 | 28.48m, 5.19 $^{\circ}$ | 18.45m, 2.08 $^{\circ}$ | 51.05m, 6.41 $^{\circ}$ | 38.47m, 5.36 $^{\circ}$ | 32.16m, 5.40 $^{\circ}$ | 28.57m, 7.99 $^{\circ}$ | 13.81m, 1.53$^{\circ}$ |
| FULL7 | 17.62m, 3.95 $^{\circ}$ | 14.84m, 2.17 $^{\circ}$ | 80.29m, 6.51 $^{\circ}$ | 54.59m, 4.56 $^{\circ}$ | 47.79m, 5.44 $^{\circ}$ | 36.86m, 5.17 $^{\circ}$ | 9.81m, 1.27$^{\circ}$ |
| FULL8 | 23.59m, 5.87 $^{\circ}$ | 16.39m, 2.26 $^{\circ}$ | 111.24m, 12.78 $^{\circ}$ | 77.57m, 9.74 $^{\circ}$ | 51.93m, 7.73 $^{\circ}$ | 58.63m, 8.53 $^{\circ}$ | 11.51m, 1.34$^{\circ}$ |
| FULL9 | 13.71m, 2.57 $^{\circ}$ | 13.60m, 1.86 $^{\circ}$ | 45.50m, 3.96 $^{\circ}$ | 26.16m, 2.56 $^{\circ}$ | 14.93m, 2.84 $^{\circ}$ | 10.67m, 2.88 $^{\circ}$ | 9.51m, 1.07$^{\circ}$ |
| Average | 20.85m, 4.40 $^{\circ}$ | 15.82m, 2.09 $^{\circ}$ | 72.02m, 7.42 $^{\circ}$ | 49.20m, 5.49 $^{\circ}$ | 36.70m, 5.35 $^{\circ}$ | 33.68m, 6.14 $^{\circ}$ | 11.16m, 1.30$^{\circ}$ |

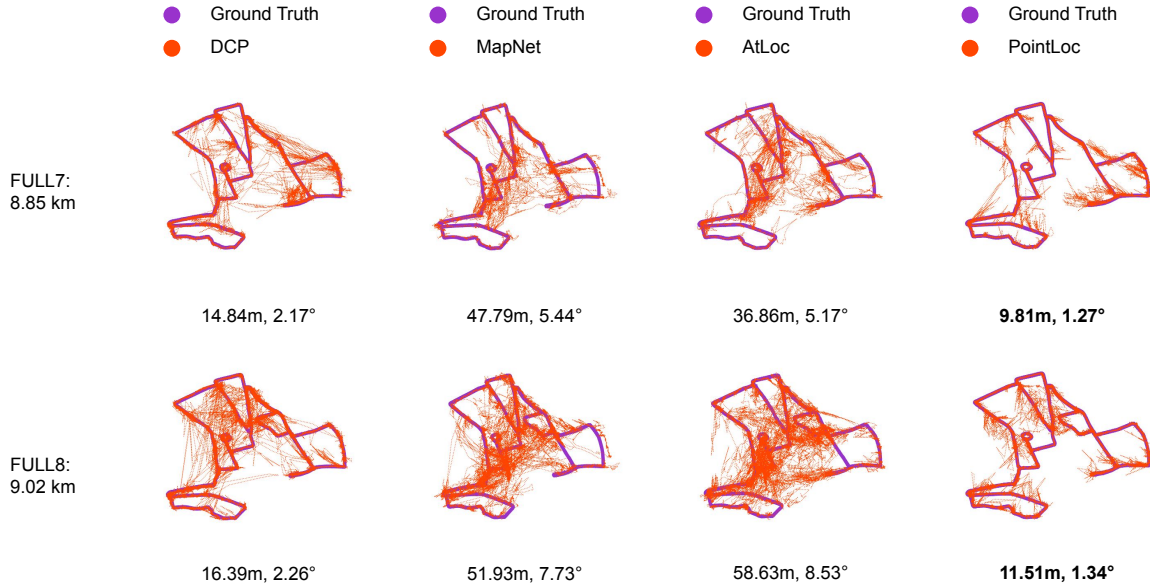


Figure 3. Trajectories of DCP, MapNet, AtLoc and the proposed PointLoc on FULL7 and FULL8 with mean translation error (m) and rotation error ($^{\circ}$). The darkorchid line is the ground truth poses, and the orange-red dot line shows the estimated poses. Our PointLoc outperforms the existing LiDAR and camera relocalization approaches by a significant margin.

Table 8. Comparisons of the computational time and storage space of PointLoc and PointNetVLAD.

| | Computational Time | Storage Space |
|--------------|--------------------|--|
| PointLoc | 0.0985 sec | 13 MB |
| PointNetVLAD | 38.0242 sec | 283 MB (76 MB model size and 207 MB reference db size) |

fectively learn meaningful features for relocalization. Furthermore, the proposed PointLoc consistently outperforms the camera relocalization baselines by a large margin. The results demonstrate that instead of utilizing RGB images as the sensory input, LiDAR point cloud can significantly improve the relocalization accuracy. Our pose predictions are even better than the sequential approaches like MapNet. In addition, the variance of learning-based camera relocalization is much larger than our approach. Therefore, PointLoc can have stable estimation across the test dataset, which indicates that the point cloud relocalization method is more robust than the visual relocalization.

6.4. Results on a Real-World Indoor Robot

We also validate our proposed PointLoc on the real-world indoor robot dataset. Our experimental design simulates the real-world scenarios of robot movements like service robots inside a large shopping mall. The robot moved forward and backward, halting when it faces obstacles. Data was collected under three conditions: static environment, one-person walking, and two-persons walking. We named the collected dataset vReLoc since it was acquired in a Vicon room for indoor relocalization task. It includes in total 18 robot movement sequences in an indoor Vicon environment. vReLoc will be released to help support future work on relocalization.

The median errors and trajectories of test results using our PointLoc are plotted in Fig. 4. The results demonstrated that PointLoc can be successfully applied to the real-world indoor scenarios for robot localization.

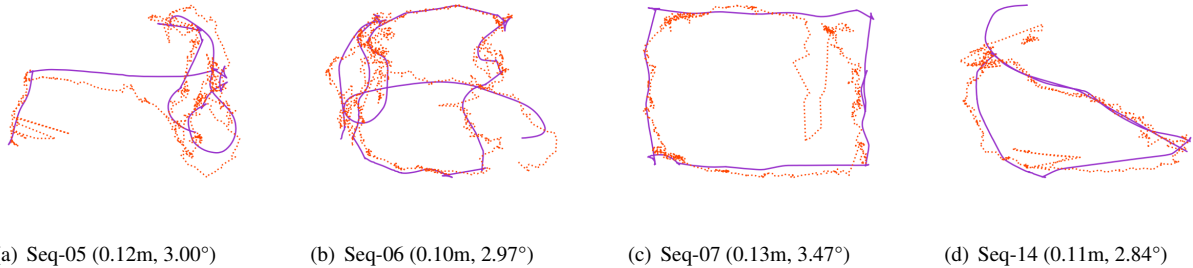


Figure 4. Trajectories of the proposed PointLoc on the vReLoc test dataset with median translation error (m) and rotation error (°). The darkorchid line is the ground truth poses, and the orange dot line is the estimated poses.

Table 9. Ablation study on the Oxford Radar RobotCar.

| Scene | PointLoc w/o Self-Attention Module | PointLoc |
|---------|------------------------------------|----------------|
| FULL6 | 15.24m, 1.95° | 13.81m, 1.53 ° |
| FULL7 | 11.32m, 1.72° | 9.81m, 1.27° |
| FULL8 | 13.63m, 1.80° | 11.51m, 1.34° |
| FULL9 | 11.03m, 1.41° | 9.51m, 1.07° |
| Average | 12.10m, 1.62° | 11.16m, 1.30° |

6.5. Ablation Study

To explore the impact of the self-attention module of our PointLoc, we conducted the following ablation study. The self-attention module was removed from the architecture since we want to examine whether the noisy point features can be eliminated. In Table 9, we report results on the Oxford Radar RobotCar dataset. The results indicate that the self-attention module indeed enhances the accuracy of relocalization.

7. Conclusion

This paper presents a novel LiDAR relocalization approach, PointLoc, based on deep learning. Leveraging a point-based neural network, it achieves superior relocalization accuracy compared to LiDAR point cloud and image-based relocalization approaches. The approach can be applied to large-scale relocalization and robot navigation scenarios for meter-level localization requirements. It can also be leveraged in indoor environments or urban areas full of high-rise buildings as a complement when the GNSS is absent. For centimeter-level requirement scenarios like autonomous driving, it can serve as a coarse localization method to provide good initial pose estimates where point cloud registration and RANSAC can be applied to further improve the accuracy of relocalization. In the future, more explorations can be done for further improving the relocalization accuracy such as eliminating the noisy point features from the point cloud.

8. Acknowledgement

This work is funded by the NIST grant 70NANB17H185. 'Pervasive, Accurate, and Reliable Location-Based Services for Emergency Responders'. The authors would like to thank Dan Barnes for the discussion on the Oxford Radar RobotCar dataset.

References

- [1] D. Barnes, M. Gadd, P. Murcatt, P. Newman, and I. Posner. The Oxford Radar RobotCar Dataset: A Radar Extension to the Oxford RobotCar Dataset. *ICRA*, 2020.
- [2] I. A. Barsan, S. Wang, A. Pokrovsky, and R. Urtasun. Learning to Localize Using a LiDAR Intensity Map. *CoRL*, 2018.
- [3] S. Brahmbhatt, J. Gu, K. Kim, J. Hays, and J. Kautz. Geometry-Aware Learning of Maps for Camera Localization. *CVPR*, 2018.
- [4] F. Camposeco, A. Cohen, M. Pollefeys, and T. Sattler. Hybrid Scene Compression for Visual Localization. *CVPR*, 2019.
- [5] R. Clark, S. Wang, A. Markham, N. Trigoni, and H. Wen. VidLoc: A deep spatio-temporal model for 6-DoF video-clip relocalization. *CVPR*, 2017.
- [6] R. Clark, S. Wang, H. Wen, A. Markham, and N. Trigoni. VINet: Visual-Inertial Odometry as a Sequence-to-Sequence Learning Problem. *AAAI*, 2017.
- [7] R. Dubé, A. Cramariuc, D. Dugas, J. Nieto, R. Siegwart, and C. Cadena. SegMap: 3D Segment Mapping using Data-Driven Descriptors. *RSS*, 2018.
- [8] Y. Feng, L. Ma, W. Liu, and J. Luo. Spatio-temporal Video Re-localization by Warp LSTM. *CVPR*, 2019.
- [9] Z. Huang, Y. Xu, J. Shi, and X. Zhou. Prior Guided Dropout for Robust Visual Localization in Dynamic Environments. *ICCV*, 2019.
- [10] A. Kendall and R. Cipolla. Modelling uncertainty in deep learning for camera relocalization. *ICRA*, 2016.
- [11] A. Kendall and R. Cipolla. Geometric Loss Functions for Camera Pose Regression with Deep Learning. *CVPR*, 2017.

[12] A. Kendall, M. Grimes, and R. Cipolla. PoseNet: A Convolutional Network for Real-Time 6-DOF Camera Relocalization. *ICCV*, 2015.

[13] H. Kim, B. Liu, C. Y. Goh, S. Lee, and H. Myung. Robust vehicle localization using entropy-weighted particle filter-based data fusion of vertical and road intensity information for a large scale urban area. *RA-L*, 2017.

[14] D. P. Kingma and J. Ba. Adam: A Method for Stochastic Optimization. *ICLR*, 2015.

[15] R. Kümmerle, D. Hähnel, D. Dolgov, S. Thrun, and W. Burgard. Autonomous driving in a multi-level parking structure. *ICRA*, 2009.

[16] T. Le and Y. Duan. PointGrid: A Deep Network for 3D Shape Understanding. *CVPR*, 2018.

[17] J. Levinson and S. Thrun. Robust Vehicle Localization in Urban Environments Using Probabilistic Maps. *ICRA*, 2010.

[18] L. Liu, H. Li, and Y. Dai. Efficient Global 2D-3D Matching for Camera Localization in a Large-Scale 3D Map. *ICCV*, 2017.

[19] W. Liu, J. Sun, W. Li, T. Hu, and P. Wang. Deep learning on point clouds and its application: A survey. *Sensors*, 2019.

[20] X. Liu, C. R. Qi, and L. J. Guibas. FlowNet3D : Learning Scene Flow in 3D Point Clouds. *CVPR*, 2019.

[21] W. Lu, G. Wan, Y. Zhou, X. Fu, P. Yuan, and S. Song. DeepVCP: An End-to-End Deep Neural Network for Point Cloud Registration. *ICCV*, 2019.

[22] W. Lu, Y. Zhou, G. Wan, S. Hou, and S. Song. L3-Net : Towards Learning based LiDAR Localization for Autonomous Driving. *CVPR*, pages 6389–6398, 2019.

[23] W. Maddern, G. Pascoe, C. Linegar, and P. Newman. 1 Year, 1000km: The Oxford RobotCar Dataset. *IJRR*, 2016.

[24] I. Melekhov, J. Ylioinas, J. Kannala, and E. Rahtu. Image-Based Localization Using Hourglass Networks. *ICCV-W 2017*, 2017.

[25] T. Naseer and W. Burgard. Deep regression for monocular camera-based 6-DoF global localization in outdoor environments. *IROS*, 2017.

[26] C. R. Qi, O. Litany, K. He, and L. J. Guibas. Deep Hough Voting for 3D Object Detection in Point Clouds. *ICCV*, 2019.

[27] C. R. Qi, H. Su, K. Mo, and L. J. Guibas. PointNet: Deep Learning on Point Sets for 3D Classification and Segmentation. *CVPR*, 2017.

[28] C. R. Qi, L. Yi, H. Su, and L. J. Guibas. PointNet++: Deep Hierarchical Feature Learning on Point Sets in a Metric Space. *NeurIPS*, 2017.

[29] N. Radwan, A. Valada, and W. Burgard. VLocNet++: Deep Multitask Learning for Semantic Visual Localization and Odometry. *RA-L*, 2018.

[30] T. Sattler, Q. Zhou, M. Pollefeys, and L. Leal-taix. Understanding the Limitations of CNN-based Absolute Camera Pose Regression Chalmers University of Technology. *CVPR*, 2019.

[31] M. A. Uy and G. H. Lee. PointNetVLAD: Deep Point Cloud Based Retrieval for Large-Scale Place Recognition. *CVPR*, 2018.

[32] A. Valada, N. Radwan, and W. Burgard. Deep Auxiliary Learning for Visual Localization and Odometry. *ICRA*, 2018.

[33] F. Walch, C. H. L. Leal-taix, T. Sattler, and S. H. D. Cremers. Image-based localization using LSTMs for structured feature correlation. *ICCV*, 2017.

[34] G. Wan, X. Yang, R. Cai, H. Li, Y. Zhou, H. Wang, and S. Song. Robust and Precise Vehicle Localization Based on Multi-Sensor Fusion in Diverse City Scenes. *ICRA*, pages 4670–4677, 2018.

[35] B. Wang, C. Chen, C. X. Lu, P. Zhao, N. Trigoni, and A. Markham. AtLoc: Attention Guided Camera Localization. *AAAI*, 2020.

[36] S. Wang, R. Clark, H. Wen, and N. Trigoni. DeepVO: Towards End-to-End Visual Odometry with Deep Recurrent Convolutional Neural Networks. *ICRA*, 2017.

[37] W. Wang, M. R. U. Saputra, P. Zhao, P. Gusmao, B. Yang, C. Chen, A. Markham, and N. Trigoni. DeepPCO : End-to-End Point Cloud Odometry through Deep Parallel Neural Network. *IROS*, 2019.

[38] Y. Wang and J. Solomon. Deep closest point: Learning representations for point cloud registration. *ICCV*, 2019.

[39] Y. Wang, Y. Sun, Z. Liu, S. E. Sarma, M. M. Bronstein, and J. M. Solomon. Dynamic Graph CNN for Learning on Point Clouds. *ACM TOG*, 2019.

[40] X. Wei, I. A. Barsan, S. Wang, J. Martinez, and R. Ur-tasun. Learning to Localize Through Compressed Binary Maps. *CVPR*, 2019.

[41] F. Xue, X. Wang, Z. Yan, Q. Wang, J. Wang, and H. Zha. Local Supports Global: Deep Camera Relocalization with Sequence Enhancement. *ICCV*, 2019.

[42] B. Yang, S. Wang, A. Markham, and N. Trigoni. Robust Attentional Aggregation of Deep Feature Sets for Multi-view 3D Reconstruction. *IJCV*, 2019.

[43] Z. J. Yew and G. H. Lee. 3DFeat-net: Weakly supervised local 3D features for point cloud registration. *ECCV*, 2018.

[44] T. Zheng, C. Chen, J. Yuan, B. Li, and K. Ren. PointCloud Saliency Maps. *ICCV*, 2019.

[45] Y. Zhou and O. Tuzel. VoxelNet: End-to-End Learning for Point Cloud Based 3D Object Detection. *CVPR*, 2018.